

HandSCS: Structural Coordinate Space for Animatable Hand Gaussian Splatting

Yilan Dong¹ Wenqing Wang² Qing Wang¹ Jiahao Yang¹ Haohe Liu²

Xiatian Zhu² Gregory Slabaugh¹ Shanxin Yuan¹

¹Queen Mary University of London ²University of Surrey

{yilan.dong, qing.wang, jiahao.yang, g.slabaugh, shanxin.yuan}@qmul.ac.uk

{wenqing.wang, haohe.liu, xiatian.zhu}@surrey.ac.uk

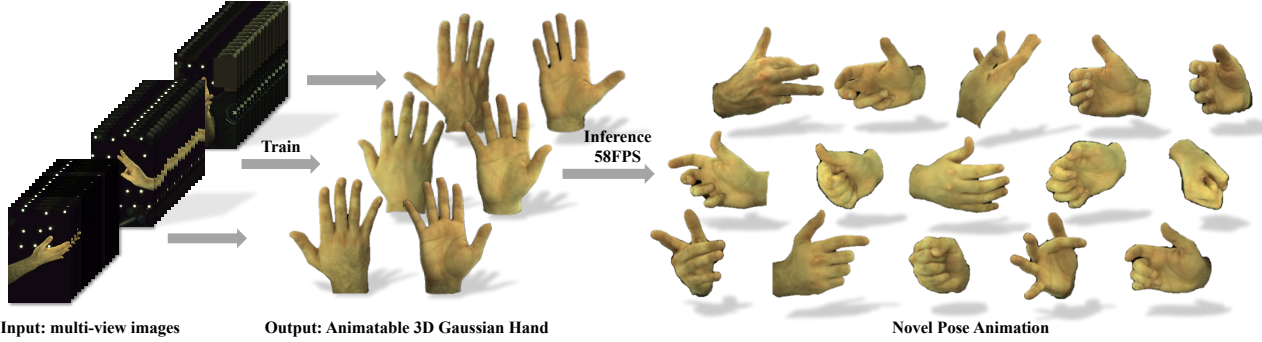


Figure 1. We introduce **HandSCS**, a structure-guided 3D Gaussian Splatting framework that provides each Gaussian with structural cues from both intra-pose and inter-pose perspectives. Intra-pose guidance is delivered through a Structural Coordinate Space that bridges sparse skeletal joints and dense Gaussians, while inter-pose guidance encourages attribute consistency across similar articulations. This formulation preserves clear boundaries and fine details, enabling high-fidelity animation even under strong deformations or self-contact.

Abstract

Creating animatable hand avatars from multi-view images requires modeling complex articulations and maintaining structural consistency across poses in real time. We present **HandSCS**, a structure-guided 3D Gaussian Splatting framework for high-fidelity hand animation. Unlike existing approaches that condition all Gaussians on the same global pose parameters, which are inadequate for highly articulated hands, **HandSCS** equips each Gaussian with explicit structural guidance from both intra-pose and inter-pose perspectives. To establish intra-pose structural guidance, we introduce a Structural Coordinate Space (SCS), which bridges the gap between sparse bones and dense Gaussians through hybrid static–dynamic coordinate basis and angular–radial descriptors. To improve cross-pose coherence, we further introduce an Inter-pose Consistency Loss that promotes consistent Gaussian attributes under similar articulations. Together, these components achieves high-fidelity results with consistent fine details, even in challenging high-deformation and self-contact regions. Ex-

periments on the InterHand2.6M dataset demonstrate that **HandSCS** achieves state-of-the-art in hand avatar animation, confirming the effectiveness of explicit structural modeling.

1. Introduction

Rendering photorealistic hands is crucial for applications such as AR/VR, immersive gaming, and human–computer interaction, requiring accurate articulation, fine appearance details, and real-time performance. Neural implicit methods [10, 22, 23] can achieve high-quality rendering but are computationally expensive and unsuitable for real-time animation. 3D Gaussian Splatting (3DGS) [15] enables efficient real-time rendering and has been extended to articulated avatars [8, 13, 19, 27, 31, 34, 35, 37, 41].

However, modeling hands remains particularly challenging due to their complex deformations, self-contact, and fine inter-finger interactions, which are less pronounced in body or head modeling. Under such highly articulated motion, Gaussians without structural awareness lack a clear

reference for their semantic role, which makes it difficult to express correct geometry and appearance. These challenges highlight the need for structure-aware modeling to preserve coherence across articulation. Yet, current 3DGS-based methods do not explicitly incorporate such structural cues, motivating us to revisit how structural guidance can be effectively integrated into the Gaussian representation. To address this, we examine structural guidance from two complementary perspectives, intra-pose guidance, which informs each Gaussian of its semantic role within a pose, and inter-pose guidance, which promotes coherent attributes across similar articulations.

For intra-pose guidance, Gaussians require a structural coordinate that distinguishes their roles within a pose. Previous works [35] conditions all Gaussians on the same pose, which provides only weak cues and can lead to over-smoothed representations, thus fail to capture the complex articulations of the hand. To this end, we propose a Structural Coordinate Space (SCS) that explicitly bridge the representation gap between sparse skeletal joints and dense Gaussian points. The SCS is composed of two tightly coupled components: coordinate basis and coordinate transformation. We use pose-dependent bone vectors as the coordinate basis and construct a hybrid structure composed of pre-defined static bones and pose-adaptive dynamic bones. The static bones preserve the overall anatomical structure, while the dynamic bones provide finer, pose-specific local guidance. Building on this basis, the Coordinate Transformation maps each Gaussian into the structural coordinate space by computing its angular and radial relations to the bone vectors. These angular–radial descriptors vary smoothly with spatial position, enabling the sparse skeletal information to be propagated to all Gaussians while preserving meaningful geometric correspondence. SCS achieves strong discrimination by leveraging the geometrically sensitive angular–radial descriptors, with the hybrid basis further enhancing this separability via pose-dependent variation.

From an inter-pose perspective, similar poses should lead to similar geometric and appearance characteristics in the rendered results. At the level of Gaussians, this implies that Gaussians in corresponding areas of the hand should maintain similar attributes under similar articulations. However, standard 3DGS optimization is performed independently for each frame and does not impose such cross-pose consistency. To ensure such coherence, we introduce an Inter-Pose Consistency Loss that promotes consistent Gaussian attributes across similar articulations.

The contributions of this paper are as follows:

1. We model structural guidance for animatable hand Gaussian Splatting from both intra- and inter-pose perspectives, enabling comprehensive structural representation and consistency across articulations.
2. We propose a Structural Coordinate Space for intra-pose

guidance that bridges sparse bones and dense Gaussians using a static–dynamic basis with angular–radial descriptors, and introduce an Inter-Pose Consistency Loss that regularizes Gaussian attributes across poses.

3. Experiments on the InterHand2.6M dataset demonstrate that HandSCS achieves state-of-the-art in hand avatar animation effectively modeling fine-grained hand structures while maintaining real-time rendering speed.

2. Related Work

2.1. Mesh based Hand Avatars

Parametric meshes are widely used for hand avatar modeling [3, 5, 6, 12, 14, 20, 24, 26, 32, 33, 36] due to their explicit geometry and compatibility with animation pipelines. Early works [3, 24] estimate colored meshes, but lack fine-grained appearance. Recent methods enhance realism by incorporating appearance modeling: AMVUR [12] introduces attention-based vertices and occlusion-aware texture regression; NIMBLE [20] builds a non-rigid model with bones, muscles, and physically-based skin; HTML [33] extends MANO [36] with a PCA-based texture model; and HARP [14] adds explicit albedo and normal maps. However, these methods often rely on dense surface capture, non-rigid tracking, or subject-specific templates, increasing cost and limiting scalability.

2.2. Neural Rendering for Hand Avatars

Neural implicit representations [10, 22, 23] have been widely adopted for animatable hand avatar. Many methods [2, 4, 7, 9, 16, 29, 43] render hands via inverse LBS and volume rendering of predicted color and density fields. LISA [4] predicts per-bone color and signed distance fields; HandAvatar [2] adds explicit albedo and illumination modeling; HandNeRF [7] introduces hand-specific deformation fields. While producing high-quality results, these methods suffer from slow rendering due to dense ray sampling. To improve efficiency, mesh-guided acceleration has been explored [9, 29], though PHRIT [9] remains slow (10 FPS) and LiveHand [29] sacrifices realism for speed. OHTA [43] and BiTT [16] reconstruct relightable, personalized appearance from a single image, but struggle to maintain consistency across poses and viewpoints.

2.3. 3DGS based Hand Avatars

3D Gaussian Splatting (3DGS [15]) provides a new paradigm for real-time scene reconstruction, and has been adept at representing hand avatars by modeling geometry and appearance through continuous and differentiable Gaussian primitives [13, 31, 41]. 3D-PSHR [13] incorporates albedo and shading into the Gaussian representation, but lacks the ability to model pose-dependent appearance. GaussianHand [41] improves rendering qual-

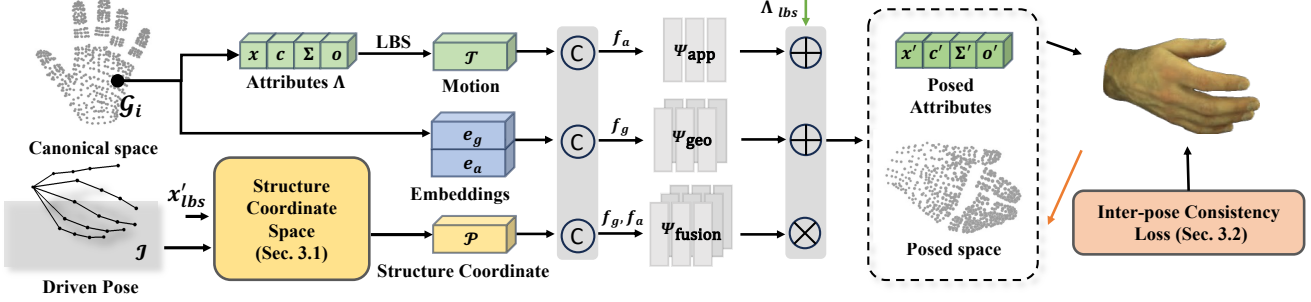


Figure 2. **Overview of HandSCS.** Each 3D Gaussian is modeled in canonical space. At the intra-pose level, we extract the LBS transformation as motion embedding \mathcal{B} , and rigidly posed position x'_{lbs} , which is combined with skeleton joints to compute the bone-relative positional embedding \mathcal{P} . Together with disentangled geometry e_g and appearance e_a embeddings, these features are used to predict adaptive attribute offsets. At the inter-pose level, a structure-consistency loss encourages consistent attributes across poses. At the point level, a neighborhood-aware densification strategy improves point distribution in under-reconstructed regions.

ity by learning Gaussian offsets from pose-dependent and pose-independent properties with a UNet-based appearance decoder. However, existing approaches do not explicitly model the underlying hand structure, limiting their ability to maintain stable geometry and appearance under challenging cases involving large articulations.

2.4. 3DGS based Human Avatars

Recent works have explored animatable human avatars using 3D Gaussian Splatting [8, 11, 17, 18, 21, 28, 30, 35, 37, 39, 42, 44]. Some methods [8, 17, 37, 39] reconstruct avatars from monocular or multi-view videos, but do not explicitly model pose-dependent appearance. To address this, several approaches [28, 35] learn Gaussian property offsets via a MLP, conditioned on the pose along with either positions [35] or per-Gaussian latent codes [28]. These methods have demonstrated promising results for clothed human bodies, which often involve challenges such as loose garments and topology variation. However, hand modeling introduces different difficulties, including high articulation, self-occlusion, and inter-part contact, highlighting the need for structure-aware modeling, which prior Gaussian-splatting avatars have not explored.

3. Method

Fig. 2 shows the framework of our method. We model a 3D hand in a canonical space, where each vertex in the MANO mesh is initialized as a 3D Gaussian. Each Gaussian \mathcal{G} is parameterized by a set of attributes $\Lambda = \{x, \Sigma, c, o\}$, representing its position, covariance matrix, color and opacity. To incorporate structural information, we introduce two complementary components. At the intra-pose level, we introduce a Structural Coordinate Space (SCS) that consist of two component, coordinate basis (Sec. 3.1.1) and coordinate transformation (Sec. 3.1.2), which help bridging the sparse skeleton joint and dense Gaussian primitives. At the inter-pose level, a Inter-Pose Consistency Loss is proposed

to regularize the geometry and appearance of corresponding Gaussians across similar articulations (Sec. 3.2). Together, these components yield a structure-aware hand model capable of high-fidelity reconstruction, pose generalization, and stable real-time rendering.

3.1. Structural Coordinate Space

3.1.1. Structural Coordinate Basis

We construct a unified set of *static* and *dynamic* bones vector to define the structural coordinate basis of the SCS. The static bones capture the unified physical hand structure and are deformed through the standard LBS in MANO model, while preserving a consistent canonical skeletal topology across poses. In contrast, the dynamic bones adaptively model pose-dependent structural variations. Together, they form a flexible structural coordinate basis.

Static Bone Basis. The static part defines the physical hand bones derived from the MANO kinematic model [36], augmented with cross-finger connections to capture anatomical relationships between adjacent fingers. To maintain a compact topology, we remove redundant wrist-to-finger edges for all fingers except the thumb. The resulting static bone topology is formulated as

$$\mathcal{E}_s = (\mathcal{E}_{\text{MANO}} \setminus \mathcal{E}_{\text{removed}}) \cup \mathcal{E}_{\text{cross}}, \quad (1)$$

Given the pose parameters θ and shape parameters β , the MANO model computes the joint positions in observed space $\mathcal{J}_o = \{j_o^i\}_{i=0}^{K-1}$, where $\mathcal{J}_o \in \mathbb{R}^{K \times 3}$ and K is the number of joints. Using the defined topology $\mathcal{E}_{\text{static}} = \{(u, v) \mid v \in \mathcal{J}\}$, where u denotes the parent joint of v . The set of static bones is formulated as,

$$\mathcal{B}_s = \{\mathbf{b}_{u,v} = (j_o^u, j_o^v) \mid (u, v) \in \mathcal{E}_s\}, \quad (2)$$

Here, “static” refers to the fixed skeletal topology.

Dynamic Bone Basis. The predefined static bone alone cannot fully capture the structural variations induced by

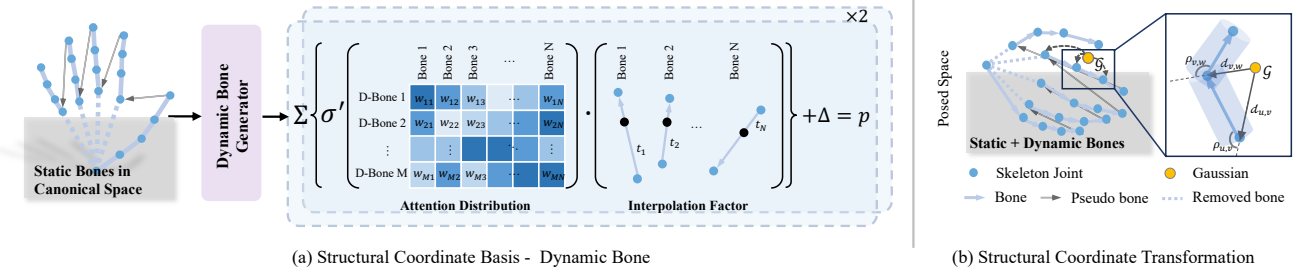


Figure 3. Illustration of **Structural Coordinate Space** (SCS). The left part shows the extended kinematic topology \mathcal{E} based on MANO model, with added cross-finger pseudo-bones and removal of redundant connections. The right part illustrates how each Gaussian is encoded with its cosine of angle $\rho_{u,v}$ and distance $d_{u,v}$ relative to each bone in the posed space.

highly articulated or interacting poses. To address this limitation, we introduce dynamic bones, constructed by referencing the static bones and interpolating their endpoints along bone segments.

Formally, given the static bone topology $\mathcal{E}_{\text{static}}$ and the canonical joint locations $\mathcal{J} = \{j^i\}_{i=0}^{K-1}$, we can obtain the set of canonical static bones as $\mathcal{B}_s^c = \{(j^u, j^v) \mid (u, v) \in \mathcal{E}_{\text{static}}\}$. The dynamic bone \mathcal{B}_d is represented by two endpoints (p, q) . For dynamic bone i , the model (i) predicts an attention distribution w over all static bones to identify relevant reference regions, and (ii) learns interpolation factors t and offsets Δ for to determine precise start and end positions. The endpoints are computed as,

$$\begin{aligned} p &= \sum_b^B \tilde{w}_b^s [(1 - t_b^s) \mathbf{j}^u + t_b^s \mathbf{j}^v] + \Delta p_b, \\ q &= \sum_b^B \tilde{w}_b^e [(1 - t_b^e) \mathbf{j}^u + t_b^e \mathbf{j}^v] + \Delta q_b, \end{aligned} \quad (3)$$

where \tilde{w}_b^s and \tilde{w}_b^e are the attention weights over canonical static bones, and $t^s, t^e \in [0, 1]$ denote the interpolation factors along each bone, and Δp and Δq are pose-dependent offsets for fine-grained adjustments. The final structural coordinate basis is obtained as $\mathcal{B} = \mathcal{B}_s \cup \mathcal{B}_d$ and the topology is $\mathcal{E} = \mathcal{E}_s \cup \mathcal{E}_d$.

To encourage smooth transitions between adjacent bones, we apply a smoothing kernel to the attention distribution. Given the attention logits $\mathcal{W} = \{w_b \mid b \in \mathcal{E}_{\text{static}}\}$, the smoothed weights are computed as

$$\tilde{\mathcal{W}} = \frac{K \sigma(\mathcal{W})}{\|K \sigma(\mathcal{W})\|_1} \quad (4)$$

where $\sigma(\cdot)$ denotes the softmax operation, and $K \in \mathbb{R}^{B \times B}$ is a fixed topology-aware smoothing kernel defined over the static hand bone, assigning a weight of 0.5 to each bone itself, 0.25 to its directly connected neighbors and 0 to to all other bones.

In practice, we generate M virtual bones using a lightweight MLP as the dynamic bone generator. The network takes the pose parameters θ and canonical joint positions \mathcal{J} as input, and outputs the parameters $w^s, w^e, t^s, t^e, \Delta p, \Delta q$. The resulting virtual bones are then combined with the static ones to form an enriched structural prior, providing a more flexible coordinate basis.

3.1.2. Structural Coordinate Transformation

The Coordinate Transformation maps Gaussian centers into the structural space in a manner that reflects their geometric relations to the underlying skeletal structure.

Per-bone structural relations. Let \mathbf{x}'_{lbs} denote the LBS-posed center of a Gaussian. The structural relation between \mathbf{x}'_{lbs} and the coordinate basis \mathcal{B} is decomposed into an *angular* term and a *radial* term. The angular term measures how the Gaussian is oriented with respect to the bone. For each bone $\mathbf{b}_{u,v} = (j^u, j^v)$, we define the Gaussian-to-basis vector $\mathbf{r}_{u,v} = \mathbf{j}_u - \mathbf{x}'_{\text{lbs}}$, we use the cosine similarity between $\mathbf{r}_{u,v}$ and $\mathbf{b}_{u,v}$,

$$\rho_{u,v} = \frac{\mathbf{r}_{u,v} \cdot \mathbf{b}_{u,v}}{\|\mathbf{r}_{u,v}\|_2 \|\mathbf{b}_{u,v}\|_2}, \quad (u, v) \in \mathcal{E}, \quad (5)$$

where $\|\cdot\|_2$ denotes L2 norm. The radial term measures the spatial affinity between the Gaussian and the bone,

$$d_{u,v} = \exp\left(-\frac{\|\mathbf{r}_{u,v}\|_2^2}{\tau^2}\right), \quad (6)$$

where τ is the decay rate, controlling the effective influence range of each bone and set to 0.08 in our experiments. This radial weighting restricts the contribution of a bone to its local neighborhood, preventing a single bone from dominating large regions and thus avoiding global over-smoothing.

Structural coordinates. By aggregating these relations across all bones, the structural coordinate descriptor for each Gaussian is defined as:

$$\mathcal{P} = [d_{u,v} \cdot \rho_{u,v}]_{(u,v) \in \mathcal{E}}. \quad (7)$$

where $[\cdot]$ denotes concatenation. Each dimension of $\mathcal{P} \in \mathbb{R}^M$ corresponds to a structural encoding associated with one coordinate basis in the SCS.

3.1.3. Embedding-based Non-rigid Deformation

We adopt an embedding-based offset formulation to model non-rigid deformations. Each Gaussian is assigned with a geometry embedding $\mathbf{e}_g \in \mathbb{R}^d$ and an appearance embedding $\mathbf{e}_a \in \mathbb{R}^d$, which are jointly optimized through the differentiable rendering pipeline. Given the structural coordinate \mathcal{P} and per-Gaussian motion embedding \mathcal{T} from the LBS transformation, and use lightweight MLP decoders to predict attribute offsets,

$$\begin{aligned}\Delta \mathbf{x}, \Delta \Sigma &= \Psi_{\text{geo}}([\mathbf{e}_g, \mathcal{P}, \mathcal{T}]), \\ \Delta c &= \Psi_{\text{app}}([\mathbf{e}_a, \mathcal{P}, \mathcal{T}]),\end{aligned}\quad (8)$$

In addition, we fuse \mathbf{f}_g and \mathbf{f}_a via a small fusion decoder,

$$\Delta \mathbf{x}^f, \Delta \Sigma^f, \Delta c^f = \Psi_{\text{fusion}}([\mathbf{e}_g, \mathbf{e}_a, \mathcal{P}, \mathcal{T}]), \quad (9)$$

and obtain the final updated attributes,

$$\begin{aligned}\mathbf{x}' &= \mathbf{x} + \Delta \mathbf{x} + \Delta \mathbf{x}^f, \\ c' &= c + \Delta c + \Delta c^f, \\ \Sigma' &= (\Delta \Sigma^f \Delta \Sigma) \Sigma (\Delta \Sigma \Delta \Sigma^f).\end{aligned}\quad (10)$$

3.2. Inter-Pose Consistency Loss

To address the structural consistency across poses, we compare t -th iteration with the previous $(t-1)$ -th iteration during training. At iteration t , the Gaussian point cloud in posed space is denoted as $\mathcal{G}_t = \{\mathcal{G}_t^i\}_{i=1}^{N_t}$, where N_t is the number of Gaussians. Each Gaussian \mathcal{G}_t^i is associated with a pose parameter θ_t and a set of combined attributes $\mathbf{M}_t^i = (\mathbf{x}_t^i, \Sigma_t^i, \mathbf{c}_t^i, \mathbf{f}_{g,t}^i, \mathbf{f}_{a,t}^i)$, where $f = [e, \mathcal{P}, \mathcal{T}]$.

To encourage corresponding Gaussians exhibiting similar attributes under similar poses, we measure the similarity between two poses θ_t and θ_{t-1} as,

$$\omega_{t,t-1} = \exp \left(- \frac{\|\Phi_\theta(\theta_t) - \Phi_\theta(\theta_{t-1})\|_2^2}{2\delta^2} \right), \quad (11)$$

where Φ_θ is a MLP and δ refers to decay factor, which we set to 1.5. Then, we establish point-wise correspondences between \mathcal{G}_t and \mathcal{G}_{t-1} via nearest-neighbor,

$$\pi(i) = \arg \min_{j=1}^{N_t} \|\mathbf{x}_t^i - \mathbf{x}_{t-1}^j\|_2^2, \quad (12)$$

where $\pi \in \mathbb{R}^{N_t \times 1}$ is the correspondence indices \mathcal{G}_t to \mathcal{G}_{t-1} . With the above components, we formulate the consistency loss as,

$$\mathcal{L}_{\text{con}} = \omega_{t,t-1} \sum_{i=1}^{N_t} \|\mathbf{M}_t^i - \bar{\mathbf{M}}_{t-1}^{\pi(i)}\|_2^2, \quad (13)$$

Here, $\bar{\mathbf{M}}_{t-1}^{\pi(i)}$ denotes the cached attributes from a historical memory, updated via exponential moving average (EMA) over past iterations. For initialization, we set $\mathbf{M}_0^i = \bar{\mathbf{M}}_1^i$. When $\theta_t = \theta_{t-1}$, the loss naturally enforces cross-view alignment for the same pose enhancing robustness under self-occlusion and viewpoint variation.

3.3. Training Objective Function

Following other hand 3DGS-based methods [13, 31], we apply a standard RGB loss, mask loss, SSIM loss, and LPIPS loss to supervise the 3D model, defined as:

$$\mathcal{L}_{\text{base}} = \mathcal{L}_{\text{rgb}} + \lambda_1 \mathcal{L}_{\text{mask}} + \lambda_2 \mathcal{L}_{\text{SSIM}} + \lambda_3 \mathcal{L}_{\text{LPIPS}}, \quad (14)$$

where λ are loss weights. Empirically, we set $\lambda_1 = 0.1$, $\lambda_2 = \lambda_3 = 0.01$. Similar to [1], we apply a smoothness loss $\mathcal{L}_{\text{smooth}}$ on the geometry embeddings to encourage local continuity in the embedding space. The overall loss is,

$$\mathcal{L} = \mathcal{L}_{\text{base}} + \lambda_{\text{con}} \mathcal{L}_{\text{con}} + \lambda_{\text{smooth}} \mathcal{L}_{\text{smooth}}, \quad (15)$$

where λ_{con} is set to 0.01 and λ_{smooth} is set to 1.

4. Experiments

4.1. Datasets and Metrics

We conduct experiments on the widely used InterHand2.6M [25] dataset, which provides large-scale multi-view sequences of diverse hand poses. To fairly assess our method, we select right-hand sequences from three subjects: test/Capture0, test/Capture1, and val/Capture0, focusing on ROM03, ROM04, and ROM07. For novel pose rendering, we allocate the last 50 frames for testing and use the remaining frames for training. For novel view synthesis, 10 views are selected for training, 15 views are used as testing set. Detailed specifications of the selected camera views are provided in the supplementary material.

We evaluate Peak Signal-to-Noise Ratio (PSNR), Structural Similarity Index Measure (SSIM) [38] and Learned Perceptual Image Patch Similarity (LPIPS) [40] as metrics for the rendering results on full image. We use FPS to compare the rendering speed. Rrendering speed are all evaluated on a single NVIDIA A100 GPU.

4.2. Implementation details

For every MLP in decoders Ψ_{geo} , Ψ_{app} and Ψ_{fusion} share the same structure, we adopt the same architecture, consisting of a fully connected multilayer perceptron with 2 hidden layers, each containing 256 neurons, a learnable gate (initialized to zero) is included to avoid very large outputs at the beginning of training. For Gaussian initialization, we use the MANO model with 778 vertices as the initial state. The color and opacity of each Gaussian are randomly initialized. More details are provided in our supplementary materials and code (to be released upon acceptance).

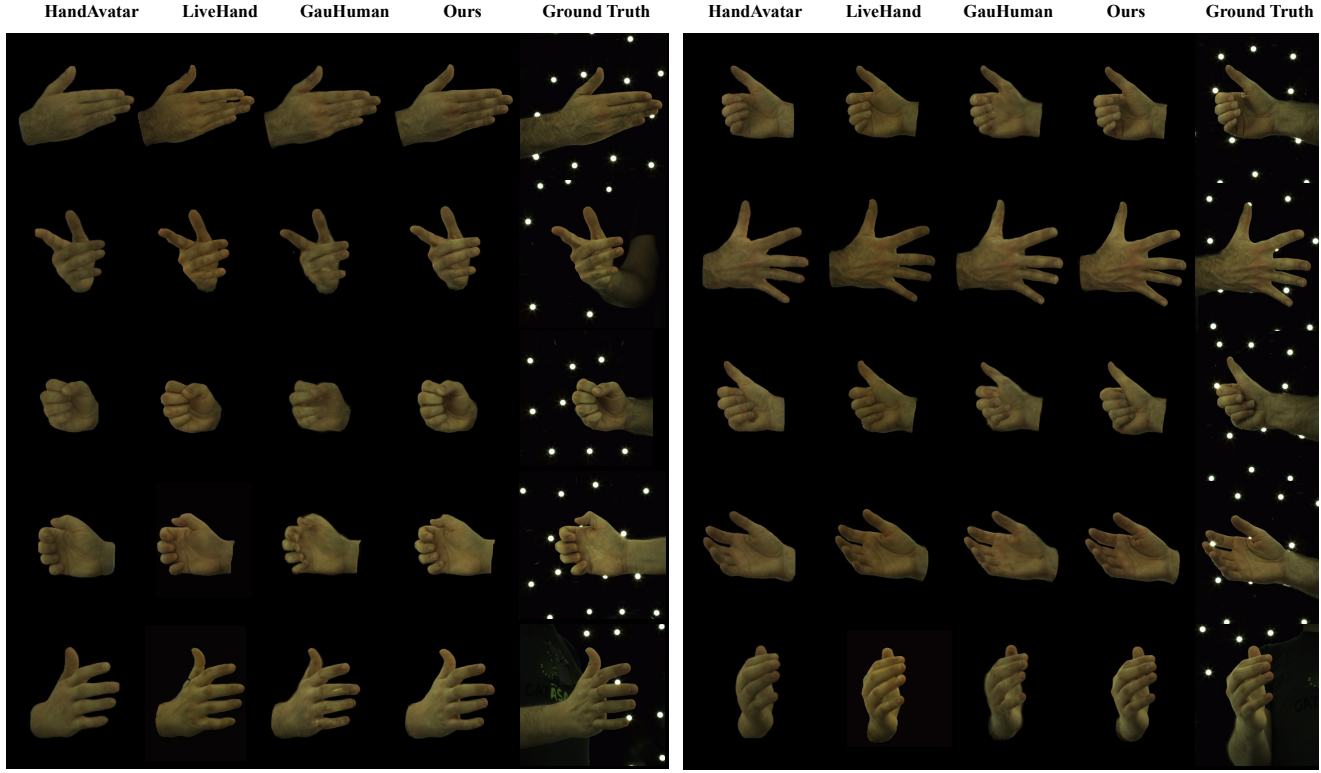


Figure 4. **Qualitative Comparison of Novel Pose Synthesis.** We compare results on InterHand2.6M [25] across three subjects using HandAvatar [2], LiveHand [29], GauHuman [8], and our method. HandSCS produces sharper structures, cleaner boundaries, and fewer artifacts under challenging articulations.

| Method | test/Capture0 | | | test/Capture1 | | | val/Capture0 | | |
|---------------------------------|-----------------|-----------------|--------------------|-----------------|-----------------|--------------------|-----------------|-----------------|--------------------|
| | PSNR \uparrow | SSIM \uparrow | LPIPS \downarrow | PSNR \uparrow | SSIM \uparrow | LPIPS \downarrow | PSNR \uparrow | SSIM \uparrow | LPIPS \downarrow |
| Novel Pose Animation | | | | | | | | | |
| LiveHand [29] | 29.17 | 0.949 | 0.0528 | 26.85 | 0.776 | 0.0619 | 29.33 | 0.893 | 0.0606 |
| HandAvatar [2] | 31.36 | 0.959 | 0.0453 | 30.37 | 0.961 | 0.0448 | 30.35 | 0.954 | 0.0499 |
| GauHuman [8] | 31.71 | 0.958 | 0.0424 | 31.72 | 0.962 | 0.0445 | 31.15 | 0.955 | 0.0488 |
| HandSCS | 32.91 | 0.966 | 0.0291 | 32.99 | 0.970 | 0.0282 | 32.40 | 0.963 | 0.0328 |
| Novel View Synthesis (10 views) | | | | | | | | | |
| LiveHand [29] | 31.95 | 0.984 | 0.0335 | 31.03 | 0.979 | 0.0367 | 30.21 | 0.969 | 0.0449 |
| HandAvatar [2] | 32.06 | 0.961 | 0.0440 | 31.62 | 0.963 | 0.0440 | 32.74 | 0.963 | 0.0432 |
| GauHuman [8] | 32.10 | 0.958 | 0.0446 | 31.37 | 0.958 | 0.0462 | 31.73 | 0.955 | 0.0479 |
| HandSCS | 35.31 | 0.973 | 0.0297 | 35.45 | 0.976 | 0.0280 | 35.77 | 0.972 | 0.0299 |

Table 1. **Quantitative comparison on InterHand2.6M [25].** For novel pose animation, HandSCS achieves the best performance across all subjects. For sparse novel view synthesis, models are trained on 10 views and evaluated on 15 held-out views. LiveHand [29] attains slightly higher SSIM due to smoother NeRF interpolation under sparse viewpoints, yet HandSCS produces sharper structures, clearer boundaries, and fewer artifacts under challenging viewing angles. Bold numbers indicate the best performance.

4.3. Baselines and Result Comparison

Baselines. To evaluate the performance of HandSCS, we conduct comparisons with state-of-the-art NeRF-based method HandAvatar [2] and LiveHand [29] and Gaussian Splatting-based methods GauHuman [8]. To ensure fairness,

we include only open-source methods and use their official implementations with default configurations. We also attempted to reproduce additional recent methods [13, 41]; however, due to missing implementation details, their reported performance could not be reliably reproduced, and

thus they are not included in our comparison.

Novel Pose Synthesis. Tab. 1 summarizes the novel pose results across three subjects. HandSCS achieves the best performance on all metrics, with average gains of +1.24 dB PSNR, +0.008 SSIM, and a 33.4% relative LPIPS reduction over the strongest baseline. These improvements are comparable to or larger than those reported in recent works [1, 2, 7, 8]. Qualitative examples in Fig. 4 show that HandSCS produces sharper details, clearer boundaries, and more stable appearance in challenging articulations. In contrast, existing methods often struggle with fine structures such as fingernails and skin textures or exhibit noticeable artifacts due to limited structural modeling.

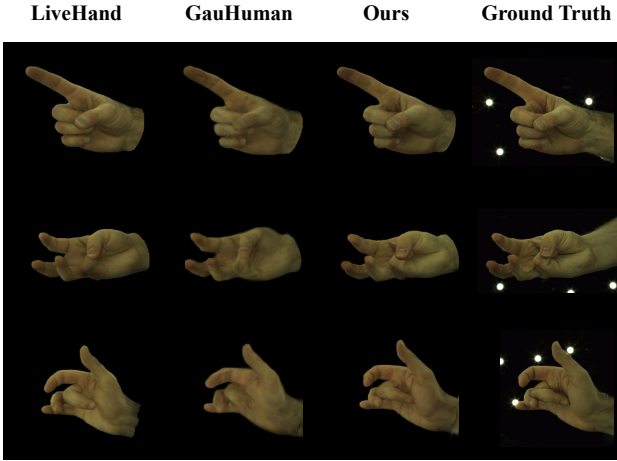


Figure 5. Qualitative comparison of novel view synthesis.

Novel view Synthesis. As shown in Tab. 1 and Fig. 5, HandSCS shows the highest rendering quality under novel viewpoints. Averaged over three subjects, HandSCS improves PSNR by +3.78 dB and SSIM by +0.017, and reduces LPIPS by 0.017 (37% relative reduction) compared with the strongest baseline GauHuman [8]. Our method preserves fine appearance details such as skin folds, fingernails, and finger boundaries, and introduces fewer artifacts in challenging regions, including occlusions and self-shadowed areas. LiveHand[29] obtains slightly higher SSIM on two subjects. This is expected, as NeRF-based methods interpolate smoothly across sparse viewpoints, while Gaussian-based models may exhibit mild color inconsistencies under difficult viewing angles. Nevertheless, HandSCS consistently produces sharper details, higher-fidelity textures, and significantly fewer rendering artifacts across views. Additional qualitative comparisons are provided in the supplementary material.

4.4. Ablation Study

We conduct ablation experiments on the InterHand2.6M dataset (subject “test/Capture0”) to assess the impact of different components, including multi-component structural

| Models | PSNR \uparrow | SSIM \uparrow | LPIPS \downarrow |
|-------------------------|-----------------|-----------------|--------------------|
| (a) baseline | 31.71 | 0.958 | 0.0428 |
| (b) Embedding+(a) | 32.23 | 0.961 | 0.0337 |
| (c) Inter-pose+(b) | 32.42 | 0.964 | 0.0335 |
| (d) SCS(Intra-pose)+(b) | 32.78 | 0.966 | 0.0301 |
| Full model | 32.91 | 0.966 | 0.0291 |

Table 2. **Ablation study on multi-component structural guidance.** (b) introduces disentangled embeddings, and (c)–(d) further incorporate inter-pose and intra-pose (SCS) structural guidance. All components contribute measurable gains, and the full model achieves the best overall performance.

guidance, embeddings for adaptive attributes offset, and the kinematic topology in positional encoding.

Multi-component Structure Ablation. Tab. 2 shows that each component brings consistent gains and that the full model achieves the best PSNR, SSIM, and LPIPS. Beyond the numbers, the ablation indicates that structural guidance improves reconstruction across normal poses and is especially helpful in challenging cases with strong deformations or self-contact, where maintaining boundaries and fine details is most difficult. Visually, as shown in Fig. 6, the baseline shows noise, blurred boundaries, and strong artifacts in contact regions. Disentangled embeddings improve stability but still fail under large deformations. Inter-pose guidance sharpens global structure, while intra-pose guidance enhances local details such as wrinkles and fingernails. The full model combines both and yields the cleanest results with clear boundaries and minimal artifacts.

| Models | PSNR \uparrow | SSIM \uparrow | LPIPS \downarrow |
|-------------------|-----------------|-----------------|--------------------|
| w/o Intra-pose | 32.42 | 0.9636 | 0.0335 |
| w/o Static Bones | 32.64 | 0.965 | 0.0302 |
| w/o Dynamic Bones | 32.70 | 0.965 | 0.0311 |
| Full model | 32.91 | 0.966 | 0.0291 |

Table 3. **Ablation study on coordinate basis.** w/o Intra-pose serves as the baseline to evaluate the gains from static and dynamic bones. Both components contribute complementary improvements, and the full model achieves the highest performance.

Coordinate Basis. To understand the role of the coordinate basis, we analyze the behavior of static and dynamic bones individually. Dynamic bones adapt their endpoints according to the current pose and therefore provide more localized and diverse structural cues. This flexibility allows them to better capture regions undergoing large deformations, where the sparse physical skeleton alone is insufficient to guide nearby Gaussians. As a result, dynamic bones effectively suppress artifacts such as surface glitches and broken boundaries around highly bent fingers. However, because the dynamic bones are generated without strict kine-

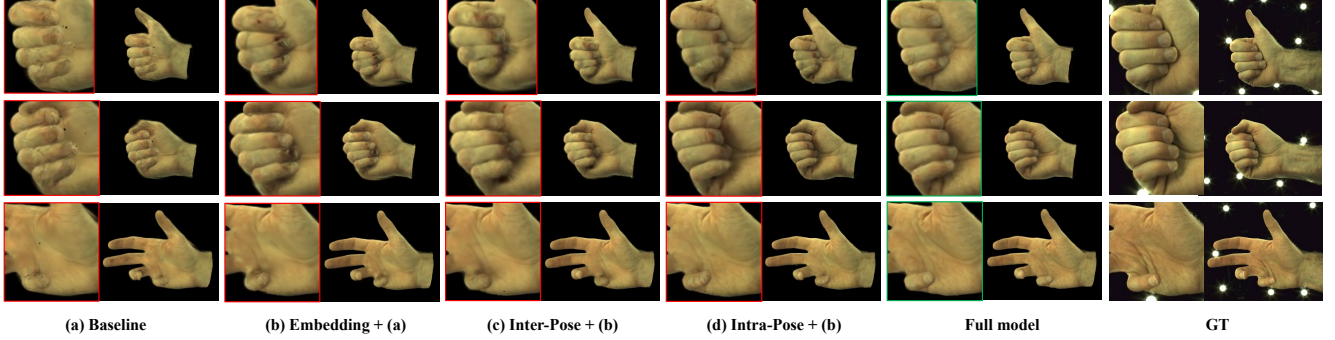


Figure 6. **Ablation study** on multi-component structural modeling. Our full model mitigates artifacts in challenging high-deformation and self-contact regions, maintaining clearer geometric boundaries and consistent fine details.

matic constraints, they may occasionally introduce pose inconsistencies or incorrect Gaussian placements. In contrast, static bones are based on the physical MANO topology and thus maintain globally coherent hand structure and correct overall pose, but their limited diversity makes them less effective in high-deformation areas, where guidance needs to be more fine-grained. Combining static and dynamic bones yields a complementary effect: static bones provide stable global structure, while dynamic bones supply expressive local cues, leading to the most robust reconstruction quality across both rigid and highly articulated hand poses.

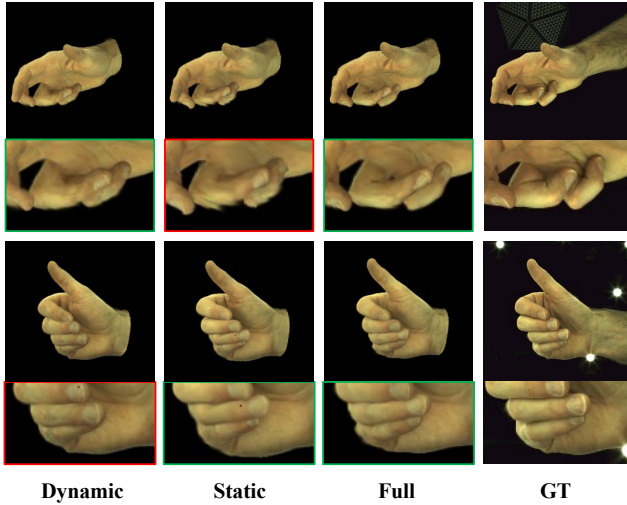


Figure 7. **Ablation study on Coordinate Basis.** Dynamic bones reduce artifacts in highly deformed areas but may cause pose errors, while static bones maintain structural correctness but are less expressive. A hybrid basis effectively integrates both strengths.

Dynamic Component Ablation. We analyze the two factors that determine how dynamic bones obtain their endpoint positions. Removing the interpolation parameter t weakens the results, as t provides continuous and smooth positioning along each bone segment. Removing the offset term Δ reduces local deformation flexibility and further compromises detail fidelity. Using both t and Δ yields com-

plementary benefits: t ensures smooth structural transitions along bone segments, while Δ enables subtle local variations around highly articulated regions. As shown in Tab. 4, combining both leads to the best reconstruction results.

| Models | PSNR \uparrow | SSIM \uparrow | LPIPS \downarrow |
|----------------|-----------------|-----------------|--------------------|
| w/o Intra-pose | 32.42 | 0.9638 | 0.0334 |
| w/o t | 32.67 | 0.9656 | 0.0300 |
| w/o Δ | 32.69 | 0.9657 | 0.0300 |
| Full model | 32.91 | 0.9663 | 0.0291 |

Table 4. **Ablation study on dynamic bones.** w/o Intra-pose serves as the baseline for evaluating the dynamic components. Removing t weakens positional alignment along bone segments, while removing Δ reduces local structural flexibility. Combining both cues yields the best performance.

5. Conclusions

We presented HandSCS, a structure-guided 3D Gaussian Splatting framework for high-fidelity hand modeling. By introducing a Structural Coordinate Space with inter-pose and intra-pose guidance, our method provides explicit geometric cues that support stable global alignment and fine-grained local detail. Experiments on InterHand2.6M show that HandSCS delivers state-of-the-art performance and cleaner visual results than existing NeRF- and Gaussian-based methods. Ablation studies further indicate that structural guidance improves reconstruction under standard poses and is especially effective in challenging cases with strong deformations or self-contact. Overall, our findings highlight the value of explicit structural modeling for articulated hands and suggest extending such guidance to full-body avatars and more complex articulated scenes.

Limitation. HandSCS still relies on the MANO model for pose initialization, which inherently constrains the expressiveness of the pose bottleneck. In our failure case analysis, we observe that certain hand articulations exhibit incorrect rendering results when the initial MANO parameters are inaccurate. Although the model does explicitly optimize

MANO pose parameters during training, these inaccuracies cannot always be fully corrected and may propagate into the final rendering results.

References

- [1] Jeongmin Bae, Seoha Kim, Youngsik Yun, Hahyun Lee, Gun Bang, and Youngjung Uh. Per-gaussian embedding-based deformation for deformable 3D gaussian splatting. In *European Conference on Computer Vision*, pages 321–335. Springer, 2024. [5](#), [7](#)
- [2] Xingyu Chen, Baoyuan Wang, and Heung-Yeung Shum. Hand Avatar: Free-pose hand animation and rendering from monocular video. In *Proceedings of the IEEE/CVF Conference on Computer Vision and Pattern Recognition*, pages 8683–8693, 2023. [2](#), [6](#), [7](#)
- [3] Yujin Chen, Zhigang Tu, Di Kang, Linchao Bao, Ying Zhang, Xuefei Zhe, Ruizhi Chen, and Junsong Yuan. Model-based 3d hand reconstruction via self-supervised learning. In *Proceedings of the IEEE/CVF Conference on Computer Vision and Pattern Recognition*, pages 10451–10460, 2021. [2](#)
- [4] Enric Corona, Tomas Hodan, Minh Vo, Francesc Moreno-Noguer, Chris Sweeney, Richard Newcombe, and Lingni Ma. Lisa: Learning implicit shape and appearance of hands. In *Proceedings of the IEEE/CVF Conference on Computer Vision and Pattern Recognition*, pages 20533–20543, 2022. [2](#)
- [5] Qijun Gan, Wentong Li, Jinwei Ren, and Jianke Zhu. Fine-grained multi-view hand reconstruction using inverse rendering. In *Proceedings of the AAAI Conference on Artificial Intelligence*, pages 1779–1787, 2024. [2](#)
- [6] Qijun Gan, Zijie Zhou, and Jianke Zhu. Xhand: Real-time expressive hand avatar. *arXiv preprint arXiv:2407.21002*, 2024. [2](#)
- [7] Zhiyang Guo, Wengang Zhou, Min Wang, Li Li, and Houqiang Li. Handnerf: Neural radiance fields for animatable interacting hands. In *Proceedings of the IEEE/CVF Conference on Computer Vision and Pattern Recognition*, pages 21078–21087, 2023. [2](#), [7](#)
- [8] Shoukang Hu, Tao Hu, and Ziwei Liu. GauHuman: Articulated gaussian splatting from monocular human videos. In *Proceedings of the IEEE/CVF Conference on Computer Vision and Pattern Recognition*, pages 20418–20431, 2024. [1](#), [3](#), [6](#), [7](#)
- [9] Zhisheng Huang, Yujin Chen, Di Kang, Jinlu Zhang, and Zhigang Tu. Phrit: Parametric hand representation with implicit template. In *Proceedings of the IEEE/CVF International Conference on Computer Vision*, pages 14974–14984, 2023. [2](#)
- [10] Boyi Jiang, Yang Hong, Hujun Bao, and Juyong Zhang. Selfrecon: Self reconstruction your digital avatar from monocular video. In *Proceedings of the IEEE/CVF Conference on Computer Vision and Pattern Recognition*, pages 5605–5615, 2022. [1](#), [2](#)
- [11] Yuheng Jiang, Zhehao Shen, Penghao Wang, Zhuo Su, Yu Hong, Yingliang Zhang, Jingyi Yu, and Lan Xu. HiFi4G: High-fidelity human performance rendering via compact gaussian splatting. In *Proceedings of the IEEE/CVF Conference on Computer Vision and Pattern Recognition*, pages 19734–19745, 2024. [3](#)
- [12] Zheheng Jiang, Hossein Rahmani, Sue Black, and Bryan M Williams. A probabilistic attention model with occlusion-aware texture regression for 3D hand reconstruction from a single rgb image. In *Proceedings of the IEEE/CVF Conference on Computer Vision and Pattern Recognition*, pages 758–767, 2023. [2](#)
- [13] Zheheng Jiang, Hossein Rahmani, Sue Black, and Bryan Williams. 3D points splatting for real-time dynamic hand reconstruction. *Pattern Recognition*, page 111426, 2025. [1](#), [2](#), [5](#), [6](#)
- [14] Korrawe Karunratanakul, Sergey Prokudin, Otmar Hilliges, and Siyu Tang. HARP: Personalized hand reconstruction from a monocular rgb video. In *Proceedings of the IEEE/CVF Conference on Computer Vision and Pattern Recognition*, pages 12802–12813, 2023. [2](#)
- [15] Bernhard Kerbl, Georgios Kopanas, Thomas Leimkühler, and George Drettakis. 3D gaussian splatting for real-time radiance field rendering. *ACM Transactions on Graphics*, 42(4), 2023. [1](#), [2](#)
- [16] Minje Kim and Tae-Kyun Kim. BiTT: Bi-directional texture reconstruction of interacting two hands from a single image. In *Proceedings of the IEEE/CVF Conference on Computer Vision and Pattern Recognition*, pages 10726–10735, 2024. [2](#)
- [17] Muhammed Kocabas, Jen-Hao Rick Chang, James Gabriel, Oncel Tuzel, and Anurag Ranjan. Hugs: Human gaussian splats. In *Proceedings of the IEEE/CVF Conference on Computer Vision and Pattern Recognition*, pages 505–515, 2024. [3](#)
- [18] Youngjoong Kwon, Baole Fang, Yixing Lu, Haoye Dong, Cheng Zhang, Francisco Vicente Carrasco, Albert Mosella-Montoro, Jianjin Xu, Shingo Takagi, Daeil Kim, et al. Generalizable human gaussians for sparse view synthesis. In *European Conference on Computer Vision*, pages 451–468. Springer, 2024. [3](#)
- [19] Mengtian Li, Shengxiang Yao, Zhifeng Xie, and Keyu Chen. Gaussianbody: Clothed human reconstruction via 3d gaussian splatting. *arXiv preprint arXiv:2401.09720*, 2024. [1](#)
- [20] Yuwei Li, Longwen Zhang, Zesong Qiu, Yingwenqi Jiang, Nianyi Li, Yuexin Ma, Yuyao Zhang, Lan Xu, and Jingyi Yu. NIMBLE: a non-rigid hand model with bones and muscles. *ACM Transactions on Graphics*, 41(4):1–16, 2022. [2](#)
- [21] Zhe Li, Zerong Zheng, Lizhen Wang, and Yebin Liu. Animatable gaussians: Learning pose-dependent gaussian maps for high-fidelity human avatar modeling. In *Proceedings of the IEEE/CVF Conference on Computer Vision and Pattern Recognition*, pages 19711–19722, 2024. [3](#)
- [22] Marko Mihajlovic, Yan Zhang, Michael J Black, and Siyu Tang. Leap: Learning articulated occupancy of people. In *Proceedings of the IEEE/CVF Conference on Computer Vision and Pattern Recognition*, pages 10461–10471, 2021. [1](#), [2](#)
- [23] Ben Mildenhall, Pratul P Srinivasan, Matthew Tancik, Jonathan T Barron, Ravi Ramamoorthi, and Ren Ng. Nerf:

Representing scenes as neural radiance fields for view synthesis. *Communications of the ACM*, 65(1):99–106, 2021. 1, 2

[24] Gyeongsik Moon, Takaaki Shiratori, and Kyoung Mu Lee. DeepHandmesh: A weakly-supervised deep encoder-decoder framework for high-fidelity hand mesh modeling. In *European Conference on Computer Vision*, pages 440–455. Springer, 2020. 2

[25] Gyeongsik Moon, Shouo-I Yu, He Wen, Takaaki Shiratori, and Kyoung Mu Lee. InterHand2.6M: A dataset and baseline for 3D interacting hand pose estimation from a single RGB image. In *European Conference on Computer Vision*, pages 548–564. Springer, 2020. 5, 6

[26] Gyeongsik Moon, Weipeng Xu, Rohan Joshi, Chenglei Wu, and Takaaki Shiratori. Authentic hand avatar from a phone scan via universal hand model. In *Proceedings of the IEEE/CVF Conference on Computer Vision and Pattern Recognition*, pages 2029–2038, 2024. 2

[27] Arthur Moreau, Jifei Song, Helisa Dhamo, Richard Shaw, Yiren Zhou, and Eduardo Pérez-Pellitero. Human gaussian splatting: Real-time rendering of animatable avatars. In *Proceedings of the IEEE/CVF Conference on Computer Vision and Pattern Recognition*, pages 788–798, 2024. 1

[28] Arthur Moreau, Jifei Song, Helisa Dhamo, Richard Shaw, Yiren Zhou, and Eduardo Pérez-Pellitero. Human gaussian splatting: Real-time rendering of animatable avatars. In *Proceedings of the IEEE/CVF Conference on Computer Vision and Pattern Recognition*, pages 788–798, 2024. 3

[29] Akshay Mundra, Jiayi Wang, Marc Habermann, Christian Theobalt, Mohamed Elgharib, et al. Livehand: Real-time and photorealistic neural hand rendering. In *Proceedings of the IEEE/CVF International Conference on Computer Vision*, pages 18035–18045, 2023. 2, 6, 7

[30] Haokai Pang, Heming Zhu, Adam Kortylewski, Christian Theobalt, and Marc Habermann. ASH: Animatable gaussian splats for efficient and photoreal human rendering. In *Proceedings of the IEEE/CVF Conference on Computer Vision and Pattern Recognition*, pages 1165–1175, 2024. 3

[31] Chandradeep Pokhriya, Ishaan Nikhil Shah, Angela Xing, Zekun Li, Kefan Chen, Avinash Sharma, and Srinath Sridhar. MANUS: Markerless grasp capture using articulated 3D gaussians. In *Proceedings of the IEEE/CVF Conference on Computer Vision and Pattern Recognition*, pages 2197–2208, 2024. 1, 2, 5

[32] Rolandos Alexandros Potamias, Stylianos Ploumpis, Stylianos Moschoglou, Vasileios Triantafyllou, and Stefanos Zafeiriou. Handy: Towards a high fidelity 3D hand shape and appearance model. In *Proceedings of the IEEE/CVF Conference on Computer Vision and Pattern Recognition*, pages 4670–4680, 2023. 2

[33] Neng Qian, Jiayi Wang, Franziska Mueller, Florian Bernard, Vladislav Golyanik, and Christian Theobalt. HTML: A parametric hand texture model for 3D hand reconstruction and personalization. In *European Conference on Computer Vision*, pages 54–71. Springer, 2020. 2

[34] Shenhan Qian, Tobias Kirschstein, Liam Schoneveld, Davide Davoli, Simon Giebenhain, and Matthias Nießner. Gaus- sianavatars: Photorealistic head avatars with rigged 3d gaussians. In *Proceedings of the IEEE/CVF Conference on Computer Vision and Pattern Recognition*, pages 20299–20309, 2024. 1

[35] Zhiyin Qian, Shaofei Wang, Marko Mihajlovic, Andreas Geiger, and Siyu Tang. 3DGS-Avatar: Animatable avatars via deformable 3D gaussian splatting. In *Proceedings of the IEEE/CVF Conference on Computer Vision and Pattern Recognition*, pages 5020–5030, 2024. 1, 2, 3

[36] Javier Romero, Dimitrios Tzionas, and Michael J. Black. Embodied hands: modeling and capturing hands and bodies together. *ACM Transactions on Graphics*, 36(6), 2017. 2, 3

[37] Zhijing Shao, Zhaolong Wang, Zhuang Li, Duotun Wang, Xiangru Lin, Yu Zhang, Mingming Fan, and Zeyu Wang. Splattingavatar: Realistic real-time human avatars with mesh-embedded gaussian splatting. In *Proceedings of the IEEE/CVF Conference on Computer Vision and Pattern Recognition*, pages 1606–1616, 2024. 1, 3

[38] Zhou Wang, Alan C Bovik, Hamid R Sheikh, and Eero P Simoncelli. Image quality assessment: from error visibility to structural similarity. *IEEE Transactions on Image Processing*, 13(4):600–612, 2004. 5

[39] Jing Wen, Xiaoming Zhao, Zhongzheng Ren, Alexander G Schwing, and Shenlong Wang. Gomavatar: Efficient animatable human modeling from monocular video using gaussians-on-mesh. In *Proceedings of the IEEE/CVF Conference on Computer Vision and Pattern Recognition*, pages 2059–2069, 2024. 3

[40] Richard Zhang, Phillip Isola, Alexei A Efros, Eli Shechtman, and Oliver Wang. The unreasonable effectiveness of deep features as a perceptual metric. In *Proceedings of the IEEE/CVF Conference on Computer Vision and Pattern Recognition*, pages 586–595, 2018. 5

[41] Lizhi Zhao, Xuequan Lu, Runze Fan, Sio Kei Im, and Lili Wang. Gaussianhand: Real-time 3D gaussian rendering for hand avatar animation. *IEEE Transactions on Visualization and Computer Graphics*, 2024. 1, 2, 6

[42] Shunyuan Zheng, Boyao Zhou, Ruizhi Shao, Boning Liu, Shengping Zhang, Liqiang Nie, and Yebin Liu. GPS-Gaussian: Generalizable pixel-wise 3D gaussian splatting for real-time human novel view synthesis. In *Proceedings of the IEEE/CVF Conference on Computer Vision and Pattern Recognition*, pages 19680–19690, 2024. 3

[43] Xiaozheng Zheng, Chao Wen, Zhuo Su, Zeran Xu, Zhaohu Li, Yang Zhao, and Zhou Xue. OHTA: One-shot hand avatar via data-driven implicit priors. In *Proceedings of the IEEE/CVF Conference on Computer Vision and Pattern Recognition*, pages 799–810, 2024. 2

[44] Wojciech Zienonka, Timur Bagautdinov, Shunsuke Saito, Michael Zollhöfer, Justus Thies, and Javier Romero. Drivable 3D gaussian avatars. *arXiv preprint arXiv:2311.08581*, 2023. 3